Rare Metal Materials and Engineering
Volume 52, Issue 10, October 2023
Available online at www.rmme.ac.cn

Science Press

Cite this article as: Ji Shouchang, Li Jinglong, Yang Haiyu, et al. Deposition Behavior of HVOF Sprayed WC-12Co Particles on AA7075[J]. Rare Metal Materials and Engineering, 2023, 52(10): 3345-3354.

ARTICLE

Deposition Behavior of HVOF Sprayed WC-12Co Particles on AA7075

Ji Shouchang[1,2,3], Li Jinglong[1,2], Yang Haiyu[3], Wang Shaopeng[3], Qiao Jiangjiang[3], Wen Qifan[3]

[1] State Key Laboratory of Solidification Processing, Northwestern Polytechnical University, Xi'an 710072, China; [2] Shaanxi Key Laboratory of Friction Welding Technologies, Northwestern Polytechnical University, Xi'an 710072, China; [3] Northwest Institute for Nonferrous Metal Research, Xi'an 710016, China

Abstract: WC-12Co particles were deposited on polished AA7075 (7075 aluminum alloy) substrate by HVOF (high velocity oxy-fuel) spraying. The microstructure, composition and hardness of the deposits were analyzed by SEM, EDS and nanoindentation hardness tester, respectively. The deposition behavior of six types of particles in three different molten states, including non-molten, semi-molten, and molten particles, was investigated. Results show that different types of particles have great impact on the substrate, which makes the AA7075 substrate deform or causes tears. The surface morphology and cross-sectional morphology of the deposits are different from those of the original powder. The surface of the deposits exhibits certain melting characteristics, and the cross-section is relatively dense. The semi-molten particles and molten particles generate some tearing to the substrate, and have a metallurgical bonding with the substrate to form a mutual meting zone. After the deposition of the particles, a hardened layer is formed on substrate surface with a thickness about 5 μm, and there is a certain gradient change in the hardness. The hardness near the surface is 3420 MPa, which is 1.56 times higher than that of the substrate (2200 MPa). The increase in hardness is originated from two factors: the peening effect of particles at high temperature and high speed, and the work hardening caused by particle extruding substrate.

Key words: HVOF; AA 7075; deposition behavior; melt; metallurgical bond; harden layer

AA7075 is an Al-Zn-Mg-Cu high strength aluminum alloy[1], which has been widely used in aircraft[2]. Its general hardness is below 1960 MPa[3–4], so it has unsatisfying tribological behavior, and still cannot meet the requirements of wear resistance. Electroplated hard Cr (EHC) treatment is often used to improve the wear resistance of workpiece contact surface. However, the disadvantages of EHC are as follows. First, there is an oxide film on the surface of aluminum alloy, which is difficult to remove completely in the electroplated process, resulting in a poor bonding between the EHC layer and aluminum substrate. Second, EHC will cause serious environmental pollution because of a large amount of carcinogenic Cr^{6+} acid and wastewater containing Cr^{6+} produced during the process.

Tungsten carbide-based cermet coatings have good wear resistance[5]. HVOF (high velocity oxy-fuel) spraying tungsten carbide-based cermet is one of the most promising alternatives to EHC[5–12]. The most applied carbide-based cermet coatings are the WC-Co coatings[13], and HVOF spraying is one of the best methods for depositing conventional WC-Co cermet powder because the powder subjected to higher velocities and lower temperatures causes less decomposition of the WC during spraying process[14]. HVOF spraying requires a higher temperature than cold spraying and a higher speed than plasma spraying. HVOF spraying deposits tungsten carbide ceramics in a molten or semi-molten state in stacks to obtain a nearly dense coating with a higher bond strength[15–16]. Particles solidification plays an important role in determining coating structure and performance[17–18]. The state of individual particles upon impact with the substrate affects the bonding strength between the coating and the substrate, and appropriate interface melting has been approved to be

Received date: June 19, 2023
Foundation item: National Natural Science Foundation of China (51975480, 52075449); Shaanxi Province Scientific and Technological Project (2022SF-294)
Corresponding author: Li Jinglong, Ph. D., Professor, Shaanxi Key Laboratory of Friction Welding Technologies, State Key Laboratory of Solidification Processing, Northwestern Polytechnical University, Xi'an 710072, P. R. China, Tel: 0086-29-86230194, E-mail: lijinglg@nwpu.edu.cn

beneficial to the particle bonding in a strong metallurgical bond forms at the interface[19].

Many scholars have studied the deposition behavior of HVOF spraying tungsten carbide ceramic particles on aluminum substrate. Bolelli[20] and Barletta[21] sprayed WC-10Co-4Cr on AA6082-T6 by HVOF; upon impact, the particles cause the Al substrate to deform and penetrate deeply into the substrate surface; the particles cannot spread and flatten extensively, and defects and pores of particles remain. Sun Ce[22] prepared a WC-12Co coating on AA6061 using HVOF, and the WC-12Co particles were embedded in the AA6061 substrate, they were not metallurgically bonded; the particles were "hemispherical" in a truncated section. Zha Bailin[23–24] investigated the effect of particle velocity and substrate temperature on the deposition behavior, and found that an increase in particle velocity will enhance the equivalent plastic strain of the particles, and the deposition process of WC-12Co particles is similar to that of cold spraying, which is embedded, and no metallurgical bonding is found between the particles and the substrate. Bansal[25] simulated the state of the sprayed impacted substrate, and found that in HVOF spraying process, significant peening stresses are generated during impact of molten and semi-molten particles on the substrate.

Sobolev[16] and Guilemany[26–27] deposited WC-12Co on Al-4%Cu substrate. Sobolev simulated the instantaneous temperature of the particles on the substrate at 1753–1813 K. Guilemany conducted calculations of the temperature at the interface, and found that the interface temperature of the aluminum substrate rises rapidly to about 1473 K and then decreases as heat flows into the substrate, so that after about 10^{-3} s the temperature has fallen to about the melting point of the aluminum (933 K).

Abbas[28] sprayed Ni powder onto both mild and stainless-steel substrates using HVOF. The result revealed an evidence of elemental interdiffusion at the splat-substrate interface, suggesting metallurgical bonding in this sample.

Although WC-12Co coatings have been prepared on AA7075 [13,29], the particle deposition behavior on the surface of AA7075 was seldom studied. Substrates have a significant influence on the deposition of tungsten carbide cermet particles [30–32]. The deposition of tungsten carbide cermet on other aluminum substrates has been reported by the above-mentioned scholars, while no one studied the WC-Co particle deposition behavior on AA7075. Therefore, the deposition behavior on AA7075 still needs to study. HVOF-sprayed WC-Co particles have different states, including molten particle, semi-molten particle, and non-molten particle, which can be readily obtained under different spraying conditions [17], but up to now, almost no one has studied the deposition state of these particles in different melt states under the same process. In this study, WC-12Co coating was prepared on AA7075 using HVOF, and the deposition characteristics of high-speed tungsten carbide particles on the substrate surface were investigated by SEM, EDS, and nanoindentation tests.

The formation process of HVOF spraying coatings can be summarized as follows: spraying materials enter a high-temperature and high-speed flame stream, which are heated to a molten or semi molten state, and then sprayed at a high speed and moderate temperature onto the surface of the pretreated substrate. After colliding with each other, the spraying droplets undergo deformation, high-speed quenching, solidification, and bonding with the substrate[14]. The collision between spraying materials and the surface of the substrate directly determines the magnitude of residual stress in the coating. Therefore, it is necessary to study the impact of spraying particles on the substrate and to find effective methods to optimize the coating performance.

1 Experiment

1.1 Materials and pretreatment

The substrate material for the experiment was AA7075 bar with a size of Φ30 mm×60 mm, which was purchased from Northeast Light Alloy Co., Ltd (Harbin, China). The samples were obtained through grinding by 150 grit, 800 girt, and 2000 grit abrasive paper, followed by polishing to mirror surface. The product was then cleaned in an ultrasonic cleaning machine using ethyl acetate and anhydrous ethanol, separately. The sample appearance to be sprayed is shown in Fig.1.

The powder for the deposition was produced by agglomerating sintering, purchased from Praxair Surface Technology (Indianapolis, IN, USA). The composition of the powder was WC-12Co (wt%, the actual content of Co is 11.69wt%), and the particle size distribution of the powder was 15–45 μm.

1.2 Samples preparation

WC-12Co particles were deposited by HVOF-LT spraying equipment whose schematic is shown in Fig. 2 (North-west Institute for Nonferrous Metal Research, Xi'an, China). In order to obtain six types of spray particles in three different molten states, we conducted a series of preliminary experiments and process parameters selection, and the process parameter are as follows: aviation kerosene as fuel gas with the flow rate of 19 L/h, high-pressure O_2 as combustion gas with the flow rate of 23×10^3 L/h, and N_2 as powder feeding gas with the flow rate of 0.1 L/h. The spray gun was held by ABB manipulator (Switzerland), the distance between the gun and sample surface was 300 mm, the angle was 90° [33], and the moving speed of the gun was 600 mm/min. The powder feeding rate was 0.5 kg/h, just spray for one time.

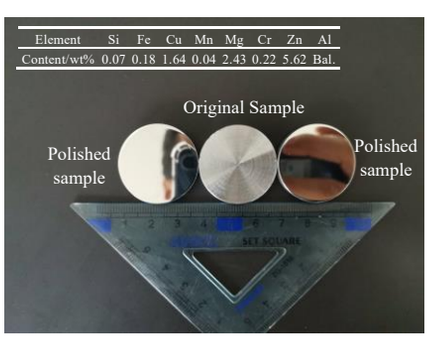

Fig.1 Sample appearance before spraying

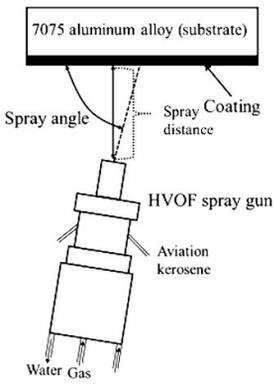

Fig.2 Schematic of HVOF spraying

The sprayed samples were cut by wire cut electrical discharge machining (WEDM, Northwest Institute for Nonferrous Metal Research, Xi'an, China), and then treated by the epoxy resin cold embedding, grinding, and polishing. Before SEM observation, the cross-section of the samples was sputtered with Pt by KYKY's SBC-12vacuum evaporation equipment (KYKY Technology Co., Beijing, China) to increase the electrical conductivity of the samples.

1.3 Characterization

The phase of the powder was determined by a D/max 2200 PC-X-ray diffractometer (XRD, Rigaku, Tokyo, Japan) under the Cu Kα radiation at 45 kV and 200 mA. XRD spectra were collected at scan rate of 10°/min and between 10° and 90°. The particle size distribution was characterized by LS13320 laser particle size analyzer (Beckman Coulter, Miami, FL, USA). The surface morphology and composition were characterized by SU 6600 field emission scanning electron microscope (FE-SEM, Hitachi, Tokyo, Japan) at an acceleration voltage of 15 kV.

The morphology and composition of the deposits were characterized by SU6600 field emission scanning electron microscopy (Hitachi Ltd. Tokyo, Japan) equipped with EDS. The nanoindentation was carried out on a Hysitron TI980 Triboindenter (Hysitron, Inc., Minnesotan, USA) with a three-sided Berkovich tip under quasi-static mode to measure the hardness.

2 Results and Discussion

2.1 Original powder

Fig. 3 shows the morphology of HVOF-sprayed WC-12Co powder. In Fig.3a, the overall sphericity of the powder is good without sharp edges. The approximately spherical shape causes good mobility of the powder, and helps the powder fly smoothly in the spraying flame. The surface of the powder is porous, which increases the specific surface area of the powder. It facilitates the heat to enter the powder during the spraying process, and the internal particles can be uniformly heated. Fig.3a_1 shows the BSE image of the complete particle, and the spherical powder is composed of different-sized WC particles (the white small particles are WC) bonded by Co. Fig. 3a_2 is the cross-sectional morphology of the powder, which exhibits porous structure, and the WC particles in the powder are evenly distributed. Fig. 3b shows morphology of an incomplete powder, which indicates that the internal and external structures of powder are almost the same.

Fig. 4 shows the XRD pattern of the sprayed powder. The main phases of WC-12Co powder are WC, Co, and no other phases are detected, such as Al, Ni.

2.2 WC-12Co particles deposited on AA7075 substrate

The deformation and deformation degree of WC-12Co

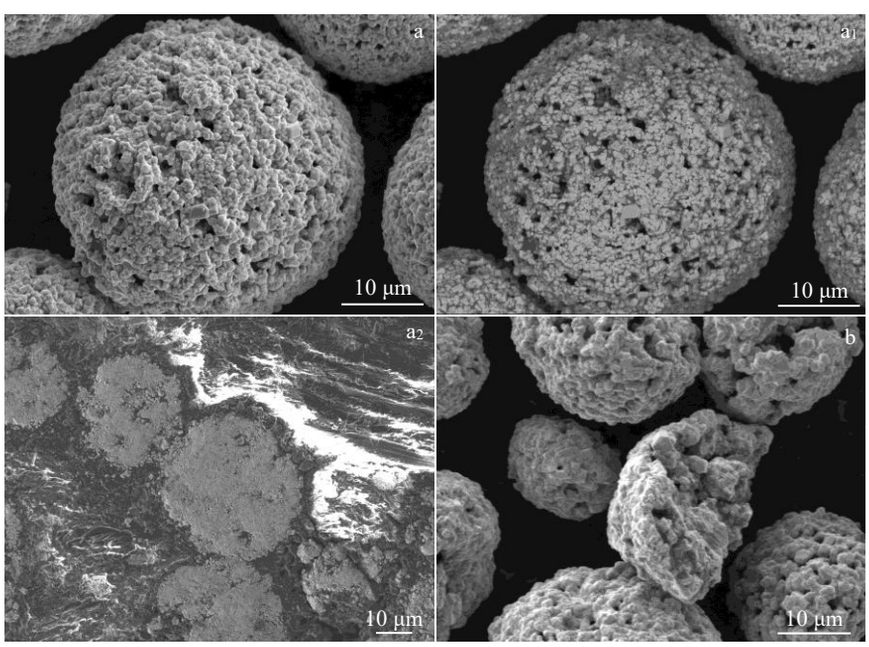

Fig.3 Morphologies of HVOF sprayed WC-Co powder: (a) SE image of intact particle, (a_1) BSE image of intact particle, (a_2) cross section of a particle, and (b) incomplete particles

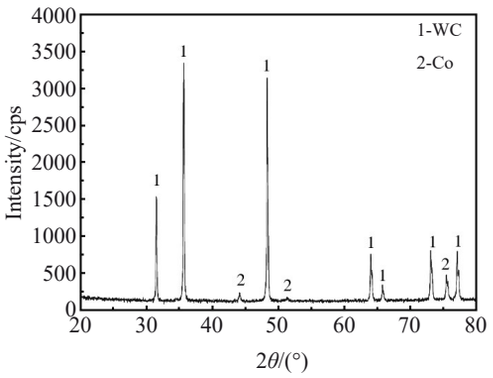

Fig.4 XRD pattern of the sprayed powder

particles have a significant effect on the deposition behavior and adhesion of WC-12Co coating on substrate. After spraying the WC-12Co powder, we observed several different deposition morphologies of particles, i. e., molten, semi-molten, and non-molten, and the deformation and deposition behavior of different powders on AA7075 substrate were analyzed.

2.2.1 Deposition analysis of non-molten particle

Fig. 5 shows the traces of the particles hitting the substrate and bouncing back. The traces retain the characteristics of the particles without remnants of WC-12Co particles. It indicates that such a particle does not reach a semi-molten or molten state but impacts the substrate at high-speed in solid state. This process produces a large extrusion deformation on the substrate, and such particles play a certain role of shot blasting on the substrate, and cause coarsening of the substrate.

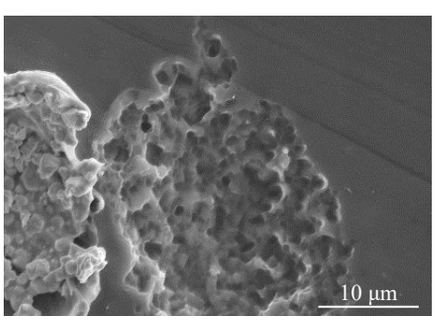

Fig.5 Morphology of WC-12Co particles after rebounding

2.2.2 Deposition analysis of semi-molten particles

(1) Spherical particle

Fig. 6 shows the shape of the deposited particles, and it can be seen from Fig. 6a that the upper part of the particle is rebounded, and extrusion appears in the lower right part of the particle; the deposited WC-12Co shows a "disk" state, which basically retains the spherical characteristics of the original WC-12Co. In Fig. 6b, the particle and the substrate are clearly divided by the extrudate, and the extrudate has an obvious protrusion, and EDS analysis confirms that the extrudate is AA7075. It is indicated that the particles have a large extrusion effect on the substrate during the depositing process and cause a large plastic deformation to the substrate. In Fig. 6c, the products in the boxed area have melt characteristics, which are different from other zone in morphology. EDS analysis shows that the content of Co is 53.49wt%; it increases greatly (compared to the original powder, 11.69wt%), and is higher than W content (46.51wt%), indicating that these products are molten.

The density of the original particles is large, because they are composed of WC besides 11.69wt% of Co binder. These large-mass particles have high kinetic energy at high velocity, so WC-12Co particles have a large impulse in the spraying impact process, exerting large impact and extrusion effect on AA7075 substrate. The hardness of WC-12Co particles is much higher than that of AA7075 substrate, so the deformation of the particles is non-coordinated plastic deformation on the AA7075 surface.

Fig. 7a shows the cross-section morphology of the deposited particle. We can see that the particle has been obviously deformed and is well combined with AA7075 substrate; the deformation is directional and gets a certain radian. There is a certain amount of extrudate at the rim of the particle. The deposited particles in Fig. 6 are basically consistent in deposition direction. Fig. 7b is the magnified morphology of the particles. The density of deposited particle is higher than that of the original powder. The upper and bottom parts of the particles are different in shape, and the bottom part features mainly the state of solidification.

As one WC-12Co particle impinges the substrate, the high impact pressure generated produces intense shear stress which deforms the particle[19]. The radian of the lower part of the deposited particles originates from the initial shape of the

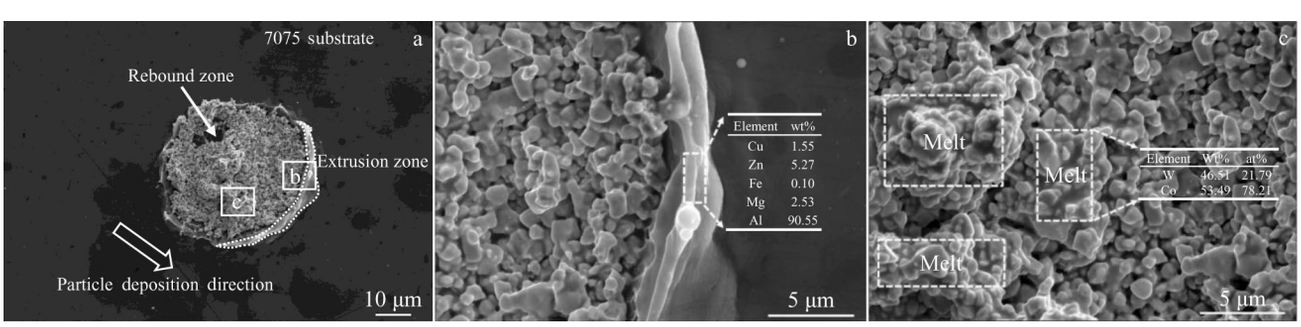

Fig.6 General (a) and enlarged (b, c) regional deposition morphologies of round particles

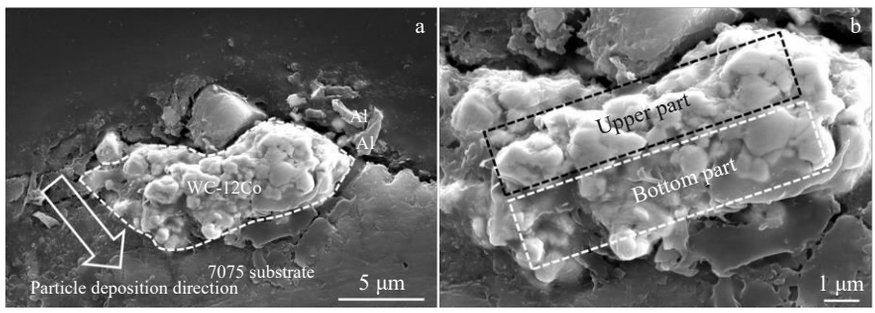

Fig.7 Cross-sectional morphologies of the particle: (a) total morphology and (b) enlarged morphology

circular tungsten carbide particles, which is basically maintained during the process of deposition and impact. The radian of the upper part is high on both sides and low in the middle. This is because the high impulse of tungsten carbide particles punches the AA7075 substrate during the deposition process. The pressure perpendicular to the bottom is the main force, while the side pressure and shear force at the edge are relatively small.

The temperature of the supersonic flame spraying process is about 2773 K, the melting point of WC ceramic particles is 3143 K, and the melting point of the bonding phase Co is only 1766 K. For the HVOF sprayed WC-Co particles, the temperature difference between the particle surface and the center is over 200 K [18], and the time for the particles staying in the flame is 3 ms. Therefore, the sprayed particles are in the state of solid-liquid coexistence (the outer surface of the particles is liquid Co, while other part of the particles is solid). During the deposition process, when the high-speed particles are deposited on the substrate, the particles are further compacted due to the reaction force in front of the particles and the high speed at the rear. The density of deposited particle is higher than that of the original powder.

The linear EDS analysis of the particle is shown in Fig.8. Al element also appears in addition to W and Co elements. Combining the EDS result and morphological characteristics, we found that W, Co and Al have fused together. It is indicated that the temperature is high enough during the deposition, it can melt aluminum substrate instantaneously, and the pores of WC-12CO particles are further filled with the molten aluminum under the high-speed impact of particles. The melting point of aluminum is about 933 K; thus, in the solid-liquid coexistence state (Co is liquid while WC is solid), aluminum substrate will be melted instantly as soon as it touches WC-12Co. When the particles impinge on the substrate, part of the kinetic energy of high-speed particles is converted into heat energy, and thus the temperature of the interface increases between the particles and the substrate [9]. As a result, under the combined action of the high temperature of particles and the heat energy of high-speed transformation, some of aluminum is fused, and aluminum and WC particles are bonded metallurgically. The metallurgical bonding increases the bonding strength between the coating and the substrate [9].

(2) Irregular particle

Fig.9a shows that the irregular particle is directional, which is embedded in the substrate and which extrudes the aluminum at the edge. The particle is semi-melted (similar to the spherical particles). There is a ribbon trace at the upper left corner range of the particle.

From Fig.9b, we can see that this trace band is significantly different from the particles in shape after rebounding (Fig.4). The direction of the band-shaped trace is indicated by the arrow, which is because this sprayed particle is deposited at a certain angle. This high-speed and high-quality particle causes tearing of the substrate and drives it to extend forward; as a result, this band-shaped trace is a sideslip zone.

In Fig.9c, melting occurs in these areas (different from the original particles), indicating that the temperature of the

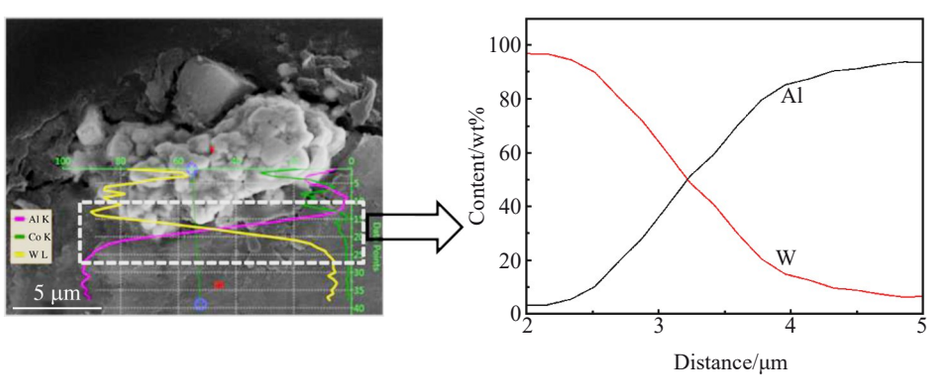

Fig.8 EDS composition analysis of particle cross-section

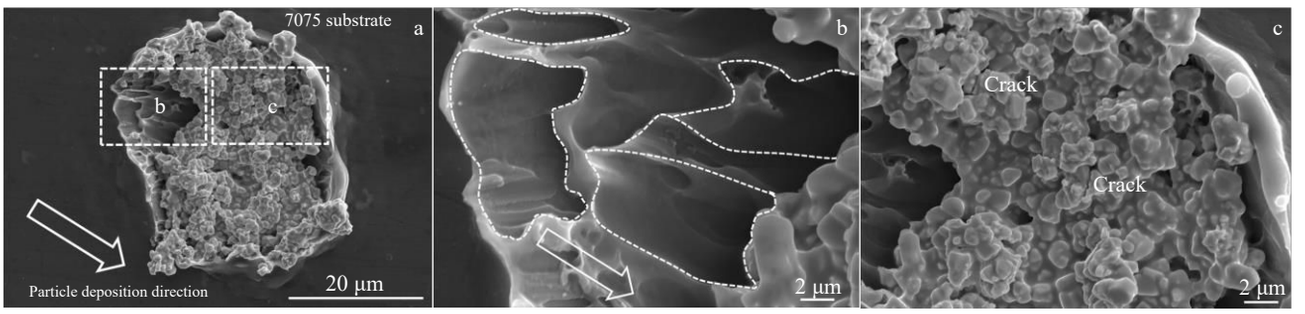

Fig.9 Irregular particle deposition morphologies: (a) general and (b, c) regional enlarged

particles in the flame flow is high enough to melt the deposited particles. There are microcracks in these zones with about 6 μm in length, and they are formed due to uneven shrinkage during the solidification process. These microcracks are short and do not penetrate the entire coating.

The hardness of the substrate cross-section after particles deposition was tested by nanoindentation method, as shown in Fig. 10. It can be seen that after depositing the particles, a hardened layer is formed and the thickness is about 5 μm, and this layer shows a gradient change in hardness. The hardness near the surface is 3420 MPa, which is 1.56 times higher than that of the substrate (2200 MPa). The increase in hardness is originated from two factors: the peening of particles and the work hardening caused by particle extrusion.

(3) Partly rebounded particle

In Fig. 11, the particle is embedded into the substrate in a certain direction; it compresses aluminum substrate along this direction, and there is a certain amount of extrudate and an extrusion zone. Some of the substrate is exposed, and the trace is the same as that of the semi-molten particle after rebounding (Fig.4), which is the rebound zone. The formation of other zones presents the melting characteristics. As shown in the BSE image, the area 1, 2, 3 is beyond the particle deposition pit, while the area 1 and 2 exhibit forward spreading of molten particle; area 3 is connected with the particle body through area 4 in the SEM image, while not connected with the particle body in the BSE image, because area 4 is extruded aluminum (EDS analysis is also aluminum), while area 3 is the splash of molten particle.

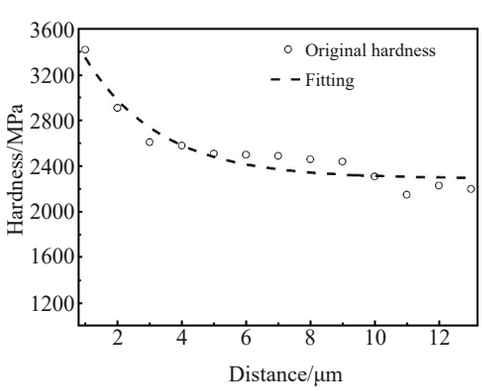

Fig.10 Variation curve of hardness with depth

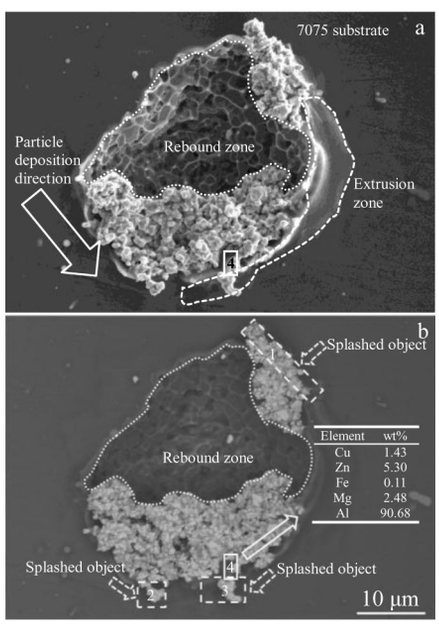

Fig.11 SE (a) and BSE (b) images of deposition morphology of semi-molten deposition particle

Fig. 12 shows the EDS analysis for the cross-section of the deposition product. Compared with the original particles, the product after deposition has melting characteristics and is denser. The EDS (perpendicular to the substrate) result shows that there is a certain fusion area for W, Co and Al, indicating that the deposition temperature is high enough to ensure the integration into the deposited particles of Al. The EDS (parallel to the substrate) result shows that the main composition is W, and the change trend of Al and Co content along the test direction is basically the same. The melting of Al in Co is easier than that in W, and some of the molten Al enters the gap of WC-12Co particles in a short time impact, and some may melt in Co.

(4) Incomplete particle

Fig. 13 shows the deposition morphology of incomplete particles. There are extrusion lines on the substrate, indicating that the particle has a large extrusion on the substrate, causing significant deformation to the substrate. Comparing SE image with BSE image, it can be seen that the region in the circle has already melted; the temperature of this area should be higher than 1766 K because the melting point of Co is about 1766 K,

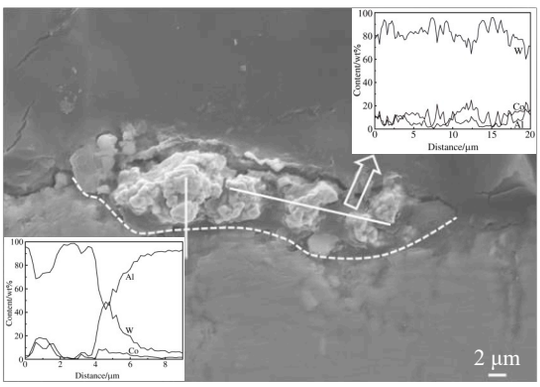

Fig.12 EDS analysis of cross-section of deposition particle

and this region is in a molten state during deposition. Compared to the SE morphology of original incomplete particles (Fig. 2), there are also obvious changes in other regions and certain melting characteristics (incomplete melting), indicating this region is in an incomplete melting state. Based on comprehensive analysis, it is concluded that a particle deposition can also show a mixed state of solid and liquid (solid-liquid state) at the same time.

(5) Deposition analysis of molten particles

In Fig. 14a, although there are certain differences between the two deposits in morphology, both are flat-shaped, in a molten state with high degree of spreading. The two deposits have splash-type features, but deposit 2 is in a certain direction. Based on Fig. 14a and Fig. 14b, the splashes are centered around the circle and appear as radioactive splashes, and they are relatively small. EDS shows that composition of the splashes is Co and Al, indicating that the WC-12Co particles are heated at a sufficiently high temperature and have already melted. During the deposition process, Co splashes out, and the molten Co melts the Al substrate. The reason for this phenomenon is that the particles are melted and deposited in the form of liquid, and spreading and splashing occur after impacting the substrate.

There are some band-shaped traces (sideslip zones) in Fig.14c and 14d, indicating that the molten particles also have a very large impulse and kinetic energy during deposition, which is enough to exert shear impact on the aluminum substrate. The direction of the side slip zones of the two deposits is slightly different (the moving direction of the spray gun during the spraying is fixed), which indicates that the

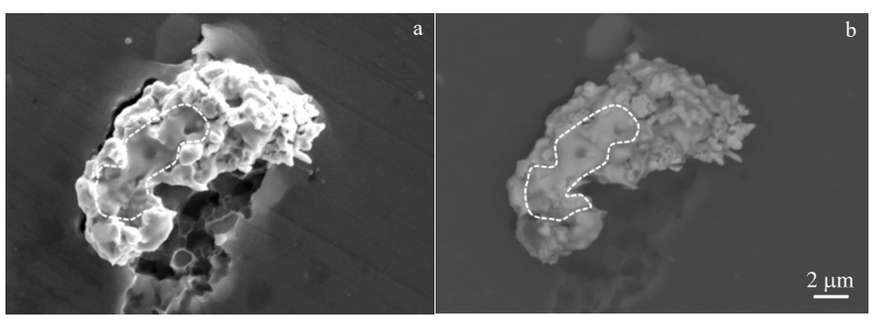

Fig.13 SE (a) and BSE (b) images of deposition morphologies of incomplete particles

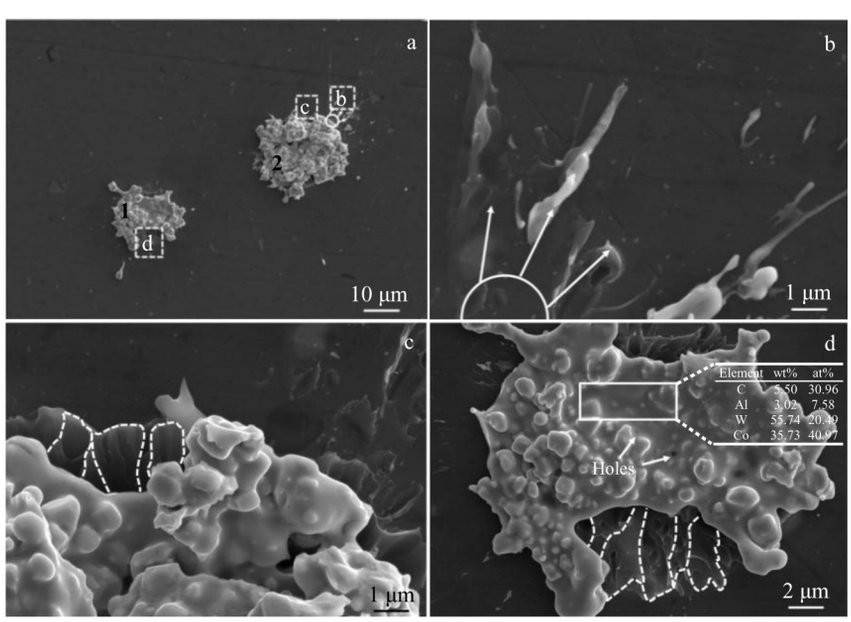

Fig.14 Deposition morphologies of sputtered tungsten carbide particles: (a) general morphology and (b–d) zoomed-in morphologies of local area

particles are not only affected by the moving direction of the spray gun, but also by their own quality during the deposition process. When the angle of the spraying to substrate is 90°, the kinetic energy of the particle impacting the substrate is the largest and the flattening effect of molten particles is optimal.

EDS analysis of the deposit shows that the content of Co is as high as 35.73%, which is significantly higher than the counterpart of 11.69% in the original powder; the content of W is 55.74%, which is obviously lower than the counterpart of the original powder. Compared to the original powder, the phenomenon of less W_xC and more Co in the deposit is due to the melting of Co, with part of W_xC particles overcoming the viscous force of the liquid Co bonder phase and rebounding, while other part of W_xC is wrapped in the molten Co.

EDS result shows that the atomic ratio of W to C is 2:3; it is possible that WC decarburizes to form W_2C substances at high temperature, or WC reacts with Co to form W_xCo_xC. Al was tested in this area, indicating that when the molten particles are sprayed onto the aluminum substrate, aluminum substrate is melted into the deposit; thus, the bonding between the deposit and the substrate is metallurgical bonding. There are circular holes in Fig.14d, which are shrinkage holes caused by the rapid solidification of molten Co.

2.3 Discussion

As is well known, the metallurgical bonding strength is much higher than mechanical bonding one, and the metallurgical bonding between deposits and substrate is the most desired in HVOF spraying. According to this experiment, temperature is one of the key factors affecting metallurgical bonding. Sobolev[16] simulated the transient temperature between them to be 1753−1813K when WC-Co is deposited onto the Al-4%Cu substrate. Guilemany[26–27] calculated the interface temperature, the temperature at the aluminum substrate at the interface rises rapidly to about 1473 K and then decreases as heat flows into the substrate so that after about 10^{-3} s, the temperature has fallen to about the melting point of the aluminum (660 °C). In this research, except for the rebound non-molten particles, the surface of deposits of four types semi-molten and molten particles have melting characteristics, indicating that these sprayed particles are heated to above 1766 K (melting point of Co) in a short time. In addition, this high temperature is conducive to the melting of particles towards the substrate, leading to diffusion from the substrate to the deposits. In general[28, 34–39], the coating prepared by HVOF involves several steps: deposition, flattening, and solidification; in this study, it is found that diffusion occurs simultaneously during the flattening and solidification processes.

It is known that a dense coating should be created by particles having sufficient kinetic energy to cause the compaction of majority of porous particle materials on which it impacts[30]. As the particle size is constant, the higher the velocity, the greater the kinetic energy of the particle. One of the factors determining the bonding between deposits and substrate is the speed of spraying particles. From the morphology of the powder particle shown in Fig. 2, fine WC particles are bonded loosely by cobalt binder, there are a large number of voids within particles, and the particles are heated and accelerated in the flame flow. Upon impact, the particles are compacted after deposition at high velocity, and near the impact area it will occur through slipping of WC particle along cobalt binder, which is referred to as the pseudo deformation of the particle[30], while the substrate is also impacted and compressed.

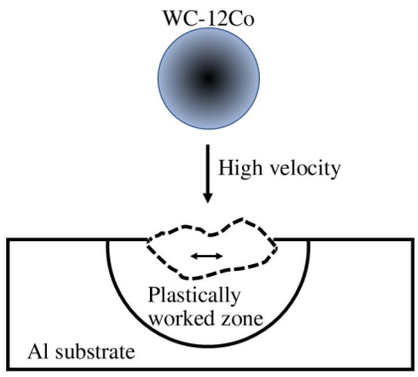

Fig.15 Schematic of influenced zone by a thermally sprayed particle

After spraying, we found that the spraying particles have “peening effect” and “work hardening effect” on the substrate. Seiji Kuroda[14] found peening effect of the HVOF sprayed particles at high velocity and in a polar molten state, and it is found that at the onset of spraying, when the substrate is peened, the peening intensity increases with the kinetic energy of sprayed particles, and compressive stress ranging from 70 to 420 MPa is generated during spraying. Because of the large difference in density and kinetic visibility between Al (2.7 g/cm^3) and WC-12Co (14.44 g/cm^3), the semi-molten WC-12Co particles with high kinetic energy have a significant peening effect on aluminum. Roy Manish[40] and Tirupataiah[41] provided the relationship between craters and hardness, i. e. the fracture diameter (W) is related to the dynamic hardness, $W=2.56rV^{1/2}(\rho_b H_d^{1/4})$, where r and H are the radius of the impact ball and the height of impacted pit, respectively, and the depth of deformation zone $d=W^2/8r$. For work hardening, the particles are heated and accelerated in a divergent flame, so the particles will have a certain deposition angle (not at 90°), these particles with high kinetic energy impact on the substrate, so there will be a certain tearing of the substate, which causes aluminum substrate to undergo a certain plastic deformation and work hardening; the schematic diagram is shown in Fig.15.

3 Conclusions

1) When the non-molten particles WC-12Co are deposited, AA7075 substrate is impacted at high speed, resulting in extrusion deformation of the aluminum substrate. After the particles are rebounded, extrusion pits remain in the substrate.

2) There are four kinds of semi-molten particles, which are spherical particles, irregular particles, partially rebounded particles and incomplete particles. When spherical particles

and irregular particles are deposited, they are partially melted. The particles have a large impact and extrusion on the substrate. The hardness of the substrate near the particles is improved. There is metallurgical bonding between the particles and the substrate. The main elements have an inter-melting zone. The particles are further compacted during the deposition process. Some rebound particles are partially melted, and the impact causes the substrate to deform. Some particles are rebounded during the deposition process, while the rest is bonded with the substrate and exhibits metallurgical bonding. Incomplete particles melt to a certain extent, and the particles have a large extrusion on the substrate, resulting in a large plastic deformation of the substrate. After the deposition of the particles, a hardened layer is formed and the thickness is about 5 μm on substrate surface, there is a certain gradient change in the hardness, and the hardness near the surface is 1.56 times higher than that of the substrate.

3) When molten particles are deposited, they impact on the substrate and spread and splash on the surface of the substrate, which is flat as a whole, and its combination with the substrate is metallurgical.

References

1 Moon Chanmi, Thuillier Sandrine, Lee Jinwoo. *Journal of Alloys and Compounds*[J], 2021, 856(5): 158 180

2 Dursun Tolga, Soutis Costas. *Materials & Design*[J], 2014, 56(4): 862

3 Ayman M Mostafa, Mohamed F Hameed, Salah S Obayya. *Journal of King Saud University-Science*[J], 2019, 31(4): 472

4 Liu Peng, Hu Jiaying, Li Huaixue *et al*. *Journal of Manufacturing Processes*[J], 2020, 60: 578

5 Grettel Navas, Giacomo D'Alisa, Joan Martínez-Alier. *Global Environmental Change*[J], 2022, 73(3): 102 474

6 Zha Bailin, Yuan Xiaojing, Wang Dewen. *Advanced Materials Research*[J], 2012, 518–523: 3984

7 Wang Qun, Luo Sisi, Wang Shaoyi *et al. International Journal of Refractory Metals and Hard Materials*[J], 2019, 81(6): 242

8 Zheng Jingwu, Chen Yishun, Fu Yongcheng *et al*. *Rare Metal Materials and Engineering*[J], 2022, 51(3): 827

9 Vuoristo P. *Thermal Spray Coating Processes*[M]. Netherlands: Elsevier Ltd Press, 2014: 229

10 Lech Pawlowski. *The Science and Engineering of Thermal Spray Coatings: Second Edition*[M]. Chichester: John Wiley & Sons, 2008

11 Ortner H M, Ettmayer P, Kolaska H *et al*. *International Journal of Refractory Metals and Hard Materials*[J], 2015, 49(3): 3

12 Vicente Albaladejo Fuentes, Ana Maria Martos, Alessio Silvello *et al*. *Encyclopedia of Materials: Metals and Alloys*[J], 2022(3): 451

13 Ba Yaer, Shen Chengjin, Ji Zhe *et al*. *Rare Metal Materials and Engineering*[J], 2022, 51(1): 166 (in Chineese)

14 Pornthep Chivavibul, Makoto Watanabe, Seiji Kuroda *et al*. *Surface and Coatings Technology*[J], 2007, 202(3): 509

15 Du Dongxing. *Effects of Surface Modification and Integrity on Fatigue Behaviors of Titanium Alloy*[D]. Xi'an: Northwestern Polytechnical University, 2014 (in Chinese)

16 Sobolev V V, Guilemany M J, Calero J A *et al*. *Journal of Thermal Spray Technology*[J], 1995, 4(4): 408

17 Sobolev V V, Guilemany J M, Garmier J C *et al*. *Surface and Coatings Technology*[J], 1994, 63: 181

18 Sun Bo, Hirokata Fukanuma. *Journal of Thermal Spray Technology*[J], 2013, 22: 263

19 Li Wenya, Cao Congcong, Yin Shuo. *Progress in Materials Science*[J], 2020, 110: 100 633

20 Bolelli G, Lusvarghi L, Barletta M. *Wear*[J], 2009, 267(5–8): 944

21 Barletta M, Bolelli G, Bonferroni B *et al*. *Journal of Thermal Spray Technology*[J], 2010, 19(1–2): 358

22 Sun Ce, Lu Guanxiong, Guo Lei *et al*. *Rare Metal Materials and Engineering*[J], 2016, 45(3): 749

23 Zha Bailin, Jia Xudong, Wang Jinjin *et al*. *Surface Technology*[J], 2020, 49(11): 101

24 Cao Xiaotian, Zha Bailin, Zhou Wei *et al*. *Surface Technology*[J], 2022, 51(6): 407

25 Bansal P, Shipway P H, Leen S B. *Journal of Thermal Spray Technology*[J], 2006, 15(4): 570

26 Guilemany J M, Nutting J, Dong Z *et al. Scripta Metallurgica et Materialia*[J], 1995, 33(7): 1055

27 Guilemany J M, Nutting J, Sobolev V V *et al. Materials Science and Engineering A*[J],1997, 232(1–2): 119

28 Abbas M, Smith G M, Munroe P R *et al*. *Surface and Coatings Technology*[J], 2020, 394: 125 909

29 Li Changjiu, Yang Guanjun. *International Journal of Refractory Metals and Hard Materials*[J], 2013, 39: 2

30 Li Changjiu, Yang Guanjun, Gao Peihu *et al*. *Journal of Thermal Spray Technology*[J], 2007, 16 (5–6): 1011

31 Couto M, Dosta S, Guilemany J M. *Surface and Coatings Technology*[J], 2015, 268(4): 180

32 Ji Shouchang, Li Jinglong, Chen Dan *et al. Rare Metal Materials and Engineering* [J], 2021,50(12): 4539

33 Mao Jie, Liu Min, Deng Ziqian *et al*. *Rare Metal Materials and Engineering*[J], 2017, 46(12): 3583

34 Chen Xiao, Li Chengdi, Gao Qinqin *et al*. *Coating*[J], 2022, 12(6): 814

35 Wolfgang Tillmann, Leif Hagen, Ingor Baumann *et al*. *Coatings*[J], 2022, 12(2): 124

36 Fan Kunyang, Jiang Wenhuang, Luzin Vladimir *et al*. *Materials*[J], 2022(15): 5537

37 Samodurova M, Shaburova N, Samoilova O *et al*. *Materials*[J], 2021,149(5):1206

38 Ingor Baumann, Leif Hagen, Wolfgang Tillmann *et al*. *Surface and Coatings Technology*[J], 2021, 405: 126 716

39 Lekatou A, Zois D, Grimanelis D. *Thin Solid Films*[J], 2008, 516(16): 5700

40 Manish Roy. *Journal of Thermal Spray Technology*[J], 2002, 11(3): 393

41 Tirupataiah Y, Venkataraman B, Sundararajan G. *Materials Science and Engineering A*[J], 1990, 124(2): 133

7075铝合金表面HVOF喷涂WC-12Co颗粒的沉积行为

姬寿长[1,2,3]，李京龙[1,2]，杨海彧[3]，王少鹏[3]，乔江江[3]，温琪凡[3]

(1. 西北工业大学 凝固技术国家重点实验室，陕西 西安 710072)

(2. 西北工业大学 摩擦焊接陕西省重点实验室，陕西 西安 710072)

(3. 西北有色金属研究院，陕西 西安 710016)

摘　要：在抛光的7075铝基体上采用HVOF（超音速火焰喷涂）沉积了WC-12Co颗粒，用SEM、EDS和纳米压痕硬度仪对沉积物的显微组织、成分和硬度进行了分析。研究了未融颗粒、未完全熔融颗粒和熔融颗粒这3种不同熔融状态下6种颗粒的沉积行为，发现不同类型的颗粒均对基体有冲击，使其发生变形或有一定的撕裂。未熔融颗粒沉积时，高速冲击铝基体使其发生挤压变形，颗粒反弹后，基体遗留挤压坑。除了反弹的未熔融颗粒，未完全熔融颗粒和熔融颗粒的沉积物与原始粉末相比，沉积物的表面形貌和横截面形貌与原始粉末不同，沉积物表面有一定的熔化特征，这是颗粒在HVOF焰流中受热温度较高使其有一定的熔融；高温高速的颗粒冲撞基体后，沉积物横截面更为致密，它们与基体之间存在冶金结合，形成了一个互熔区，表明沉积物撞击基体时温度高于铝的熔点，将铝融化并挤压进颗粒中。颗粒沉积后，在基体表面上形成一层厚度约为5 μm的硬化层，该层的硬度呈梯度变化，近表面处硬度为3420 MPa，是基体（2200 MPa）硬度的1.56倍。硬度的增加源于两个因素：高温高速颗粒的喷丸作用，及颗粒挤压基体塑形变形的加工硬化。

关键词：HVOF；7075铝合金；沉积行为；熔融；冶金结合；硬化层

作者简介：姬寿长，男，1981年生，博士生，教授，西北有色金属研究院，陕西 西安 710016，电话：029-86283410，E-mail：jscnin@163.com